Disentangling chloroplast ATP synthase regulation by proton motive force and thiol modulation in Arabidopsis leaves

Felix Buchert, Benjamin Bailleul, Pierre Joliot

Title:

Disentangling chloroplast ATP synthase regulation by proton motive force and thiol modulation in Arabidopsis leaves

Author names and affiliations:

Felix Buchert[1, 2], Benjamin Bailleul[1] and Pierre Joliot[1]

[1]Laboratory of Chloroplast Biology and Light-Sensing in Microalgae - UMR7141, IBPC, CNRS-Sorbonne Université, Paris, France.

[2] Institute of Plant Biology and Biotechnology, University of Münster, Schlossplatz 8, 48143 Münster, Germany.

Correspondence :

Felix Buchert, Institute of Plant Biology and Biotechnology, University of Münster, Schlossplatz 8, 48143 Münster, Germany,

Phone number : +49-(0)251-8324705

e-mail : f.buchert@uni-muenster.de

Abstract:

The chloroplast ATP synthase (CF_1F_o) contains a specific feature to the green lineage: a γ-subunit redox domain that contains a cysteine couple which interacts with the torque-transmitting βDELSEED-loop. This thiol modulation equips CF_1F_o with an important environmental fine-tuning mechanism. *In vitro*, disulfide formation in the γ-redox domain slows down the activity of the CF_1F_o at low transmembrane electrochemical proton gradient ($\Delta\tilde{\mu}_{H^+}$), which agrees with its proposed role as chock based on recently solved structure. The γ-dithiol formation at the onset of light is crucial to maximize photosynthetic efficiency since it lowers the $\Delta\tilde{\mu}_{H^+}$ activation level for ATP synthesis *in vitro*. Here, we validate these findings *in vivo* by utilizing absorption spectroscopy in *Arabidopsis thaliana*. To do so, we monitored the $\Delta\tilde{\mu}_{H^+}$ present in darkness and identified its mitochondrial sources. By following the fate and components of light-induced extra $\Delta\tilde{\mu}_{H^+}$, we estimated the ATP lifetime that lasted up to tens of minutes after long illuminations. Based on the relationship between $\Delta\tilde{\mu}_{H^+}$ and CF_1F_o activity, we conclude that the dithiol configuration *in vivo* facilitates photosynthesis by driving the same ATP synthesis rate at a significative lower $\Delta\tilde{\mu}_{H^+}$ than in the γ-disulfide state. The presented *in vivo* findings are an additional proof of the importance of CF_1F_o thiol modulation, reconciling biochemical *in vitro* studies and structural insights.

Keywords: chloroplast ATP synthase, electrochromic shift, redox regulation, photosynthesis, Arabidopsis, electrochemical proton gradient

Introduction

During photosynthesis, the electron transfer is coupled to a movement of protons across the thylakoid membrane, generating an electrochemical proton gradient ($\Delta\tilde{\mu}_{H^+}$) which consists of an osmotic component (the concentration gradient of hydrogen ions, ΔpH) and a membrane potential ($\Delta\Psi$). For efficient photochemistry, the $\Delta\tilde{\mu}_{H^+}$ partitioning must be dynamically regulated via thylakoid ion channels and antiporters [1, 2], as well as the chloroplast ATP synthase (CF_1F_o). The latter catalyzes the conversion of the $\Delta\tilde{\mu}_{H^+}$ into the synthesis of ATP, subsequently used in the Calvin-Benson-Bassham cycle. The enzyme consists of two portions [reviewed in 3, 4]: a membrane-spanning F_o (subunits $IV_1I_1II_1III_{14}$, or $a_1b_1b'_1c_{14}$) and a membrane-attached F_1 (subunits $\alpha_3\beta_3\gamma_1\delta_1\varepsilon_1$). In the chloroplast enzyme of vascular plants, during a 360° rotation of subunits $\gamma\varepsilon c_{14}$ against the static subunits $\alpha_3\beta_3\delta abb'$, 14 H^+ are translocated along the electrochemical gradient while 3 molecules of ATP are synthesized [5]. Perfect coupling is observed in isolated chloroplasts, i.e., H^+ slip processes do practically not occur *in vitro* [6, 7, for a different view see Ref. 8]. Being reversible, CF_1F_o catalyzes both the synthesis and hydrolysis of ATP and the reaction direction is determined by the extent of the $\Delta\tilde{\mu}_{H^+}$ and the [ATP]/([ADP][P]) ratio [9].

The activity of the CF_1F_o plays a central role in photosynthesis; it fuels the chemical phase of photosynthesis with ATP but can also, via its conductivity for H^+, participate in the regulation of the photochemical phase by modulating the osmotic component of the $\Delta\tilde{\mu}_{H^+}$ [10]. Indeed, the lumenal pH is involved in the regulation of the photosynthetic electron transfer at two levels. It regulates the photoprotective mechanism in photosystem II (PSII) [11, 12] and the turnover of the cytochrome b_6f through the so-called photosynthetic control [13]. Being at the crossroads of the dark and light phases of photosynthesis, the activity of CF_1F_o needs to be fine-tuned and, although other regulations exist [10, 14, 15], two main regulatory mechanisms can modulate the rates of the CF_1F_o. The first one is relevant for F-ATP synthase in general which is a regulation by its energy source, the $\Delta\tilde{\mu}_{H^+}$. Above a threshold value of $\Delta\tilde{\mu}_{H^+}$, the transition of the inactive CF_1F_o to a fully active form was observed in isolated chloroplasts [16, 17]. Since the structural H^+/ATP ratio (subunits c/β) differs slightly from the thermodynamic one, it is possible that a small $\Delta\tilde{\mu}_{H^+}$ fraction is lost for ATP synthesis during the CF_1F_o activation process when the membrane is energized from an equilibrated state [8]. Although the $\Delta\tilde{\mu}_{H^+}$ must contain a minimal $\Delta\Psi$ to allow for ATP synthesis at thermodynamic equilibrium [18], several studies on chloroplasts and leaves demonstrated that each of the two components of the $\Delta\tilde{\mu}_{H^+}$ can activate the enzyme if they allow the $\Delta\tilde{\mu}_{H^+}$ to reach this critical level [19-23]. We call this level $\Delta\tilde{\mu}_{H^+\,activation}$ hereafter and it can be reached by high [ATP]/([ADP][P]) ratios *in vivo*, alternatively to illumination. Specific to CF_1F_o in the green lineage is a second mechanism, "thiol modulation" or "redox regulation", which involves an insertion in the γ-subunit. The additional domain harbors a redox-active Cys couple which forms a disulfide in the dark. Formation of the γ-disulfide is, in part, mediated by a thioredoxin-like2/2-Cys peroxiredoxin redox cascade in Arabidopsis where electrons are transferred from the dithiol to H_2O_2 [24]. Dithiol formation is catalyzed by thioredoxin at moderate light intensities [25] and by NADPH thioredoxin reductase C in dim light [26, 27]. However, it is not fully understood why the redox switch evolved. An Arabidopsis mutant, termed *gamera*, remains in the γ-dithiol state in the dark by expressing a redox-insensitive γ-subunit isoform [28] and displays a stay green phenotype after several days in the dark [29]. It was suggested that altered pH-dependent protein import might partially contribute to the phenotype. The hypothesis that the slowdown of ATP hydrolysis preserves ATP in the dark [30], when the $\Delta\tilde{\mu}_{H^+}$ is low and the disulfide is present, could not explain all the phenotypes upon extended dark adaptation

[29]. Moreover, point mutants of the redox-active Cys in *Arabidopsis thaliana* are viable [31]. This suggests that the impact of thiol modulation may be more versatile than originally proposed. New discoveries regarding developmental regulation of chloroplast ATP recruitment from the cytosol [32] and photosynthetic γ-disulfide formation [24] support this view.

From a structural perspective, the γ-redox domain in the disulfide form was found to act as an ATP hydrolysis chock that is vicinal to the torque-transmitting βDELSEED-loop [33, 34], supporting earlier findings on critical γ-/β-subunit interactions during thiol modulation [35]. The redox switch also affects ATP synthesis which was first demonstrated *in vitro*. The authors showed that the dependency between the redox and $\Delta\tilde{\mu}_{H^+}$ regulations of CF_1F_o stems from a lower $\Delta\tilde{\mu}_{H^+\text{activation}}$ threshold in presence of the γ-dithiol [36], yielding half-maximal rates ~0.7 ΔpH units apart. A recent CF_1F_o structure of the γ-dithiol conformation suggests diminished torsional constraints upon reduction of the disulfide [37]. Another level of steric adjustments may be established by the $\Delta\tilde{\mu}_{H^+}$ which facilitates chemical labeling of various structurally buried residues in the γ-/β-subunit interface, including the dithiol [reviewed in 38]. Taken together, this supports the idea that CF_1F_o experiences intertwined $\Delta\tilde{\mu}_{H^+}$- and redox-dependent structural changes.

The main aim of this study is to confirm *in vitro* findings by Junesch and Gräber [36], thus stimulating further CF_1F_o thiol modulation investigations *in vivo*. It is of utmost interest to fully understand this evolutionary strategy of photosynthesis in the green lineage since the beneficial effect of thiol modulation is still under discussion while new structural insights emerge [29, 34, 37]. We differentiated between distinct redox states by using the WT and the dithiol-locked *gamera* mutant [28], in addition to an intermediate redox situation in the WT upon infiltration with the thiol reductant TCEP. Then, we obtained a $\Delta\tilde{\mu}_{H^+}$-dependent CF_1F_o activity profile in the redox states by introducing a spectroscopic technique that can also be utilized for CF_1F_o mutant characterization beyond thiol modulation.

Because the CF_1F_o activity is both $\Delta\tilde{\mu}_{H^+}$ and redox regulated, the study of its redox regulation requires the *in vivo* measurement of two parameters. First, the CF_1F_o activity which can be routinely measured since photosynthetic membranes are spectroscopic voltmeters. Accordingly, the $\Delta\Psi$ can be probed linearly by ECS, the electrochromic shift of photosynthetic pigments [39, 40, reviewed in 41]. Following a light-induced membrane energization in dark-adapted samples, the $\Delta\Psi$ (and ECS) decay is tightly linked to H^+ translocation via CF_1F_o. ECS decay kinetics following a single-turnover laser flash are therefore commonly used to probe CF_1F_o activity *in vitro* [e.g., 17] as well as *in vivo* [e.g., 28, 42]. The second parameter is the measurement of the $\Delta\tilde{\mu}_{H^+}$ extent. This is a methodological bottleneck which can be circumvented on the basis of a previous protocol [23], best explained through a simple analogy: To determine the unknown water volume in an opaque bottle one could add more water until reaching the *maximal carrying capacity*. Thus, even if the absolute value of the spillage point remains unknown, the added water volume can be quantified and expressed in relation to this reference/leak value. Regarding the measurement of the $\Delta\tilde{\mu}_{H^+}$ in the dark, Joliot and Joliot [23] have shown that a threshold of $\Delta\tilde{\mu}_{H^+}$ exists, which is a constant in a given photosynthetic material and corresponds to the leak of protons through the thylakoid membrane *in vivo* ($\Delta\tilde{\mu}_{H^+\text{leak}}$, representing the *maximal carrying capacity*). In brief, the ECS-based protocol to measure the extent of the $\Delta\tilde{\mu}_{H^+}$in the dark ($\Delta\tilde{\mu}_{H^+\text{dark}}$ hereafter) consists in energizing the membrane with a very strong light pulse and probing the ECS increase until the $\Delta\tilde{\mu}_{H^+\text{leak}}$ is reached (i.e., measuring the *remaining empty volume*).

Since this work is founded on a previously introduced method [23], we tested two implicit hypotheses *before* investigating the thiol modulation mechanism: (i) The method remains valid in

dark-adapted or illuminated leaves whatever the redox state of the γ-subunit domain, and (ii) there is no significant ΔpH generation during the short saturating pulse so that the increase of ECS (which probes $\Delta\Psi$) reflects the increase of $\Delta\tilde{\mu}_{H^+}$. After presenting the deconvolution basics first, we continue to demonstrate that those hypotheses are respected. We measure $\Delta\tilde{\mu}_{H^+}$ partitioning as a function of pulse duration and the ATP lifetime upon illumination before finally confirming that CF_1F_o is mostly in the oxidized state in dark-adapted leaves (in contrast with a previous report [23]). Validating *in vivo* the model of Junesch and Gräber, our results show that the $\Delta\tilde{\mu}_{H^+activation}$ of a disulfide-containing CF_1F_o was lowered (by $\Delta\Psi$ = 2.6 charge separations per photosystem I) and this was confirmed in leaves infiltrated with TCEP, where the efficiency of the chemical reduction of the γ-subunit was a little less than 50%.

Material and Methods

Plant material and growth conditions. The Columbia ecotype of *Arabidopsis thaliana* served as wild type in this study. The *gamera* mutant and related rescued control lines were previously published [28], and seeds were a kind gift of Dr. Jörg Meurer (Ludwig Maximilian University of Munich). Plants were grown on soil in a growth chamber under a 16-h photoperiod at 22°C (18°C at night) for about three weeks. The light intensity was set to 100 µmol photons m^{-2} s^{-1}.

Absorption changes. The experimental setup was as described previously [23]. Absorption changes were measured using a JTS spectrophotometer (Biologic). Pulses of saturating light are provided by LEDs peaking at 630 nm (~ 2500 µmol photons m^{-2} s^{-1}), unless otherwise stated. This light irradiance corresponds to ~2000 photons absorbed per second per photosystem I (PSI) or per PSII, based on the measurement of changes in the membrane potential ($\Delta\Psi$) according to the method described previously [23].

Correction and normalization of ECS signals. The light-induced membrane potential changes ($\Delta\Delta\Psi$) were measured through the absorption changes at 520 nm (reflecting mostly ECS) for experiments with short pulses (less than 20 ms), and 520 nm−546 nm for longer pulses (Fig 2). Indeed, subtracting 546 nm allows to correct for the contribution of cytochromes, P700 and scattering. However, the comparison between corrected data (520−546) and uncorrected data (520) shows that the correction was not necessary for short pulses (Fig S1). To express the measured ECS signals in charge separations per PSI, we calibrated the ECS signal by the ECS increase corresponding to one charge separation per PSI. For that, we divided all measured ECS signals in this work by ½ the ECS increase following a single-turnover flash, provided by a dye laser at 690 nm pumped with a Nd:Yag laser. Since all photosystems will generate one charge separation upon such a flash, the ECS measured 250 µs after the flash is proportional to the number of active PSI + PSII. Assuming equal concentrations of both photosystem reaction centers, half this signal is equal to the sole contribution of PSI.

Reproducibility. The kinetics of ECS rise and decay were reproducible between different leaves of different batches, but it was not the case of the extent of the ECS. This is because its amplitude depends on the density of reaction centers and ECS probes per leaf area, which slightly varied in

different cultures. For this reason, for each experiment where the amplitude of ECS was probed, we compared samples from the same batch of culture.

Chemicals and Inhibitors. We used chemical compounds by vacuum infiltration since the method did not interfere with the $\Delta\Psi$ increase and decay kinetics as compared to non-infiltrated samples (see Fig S2). All chemicals were purchased from Sigma-Aldrich. Tris(2-carboxyethyl)phosphine hydrochloride (TCEP) was dissolved in water at 0.3 M and aliquots, adjusted to pH 7.0, were frozen until further use. Solutions of antimycin-A (AA, 40 mM), nonactin (40 mM), nigericin (Nig, 10 mM) and Carbonyl cyanide 4-(trifluoromethoxy)phenylhydrazone (FCCP, 1 mM) were dissolved in ethanol and usually served as 1000x stocks that were stored at -20°C. All vacuum-infiltrated leaves were incubated in the dark for at least 15 min until measurements.

Results

1. *Following membrane potential developments during and after saturating light pulses.*

In order to study CF_1F_o in γ-disulfide- and γ-dithiol-promoting conditions, we will first elaborate on an improved protocol which is based on a previous study [23] and allows to measure the $\Delta\tilde{\mu}_{H^+}$ already present in dark-adapted leaves ($\Delta\tilde{\mu}_{H^+\,dark}$). Compared to the baseline $\Delta\Psi$ before light perturbation, the method measures $\Delta\Psi$ changes ($\Delta\Delta\Psi$) induced by a short saturating light pulse, and the return to baseline level (Fig 1). In this section, we will present the deconvolution routine of raw kinetics (ECS amplitudes and decay phases) which will be revisited below in sections 3 and 4. We make the reasonable hypothesis that short pulses (< 20 ms) induce exclusively $\Delta\Delta\Psi$ and that changes in the ΔpH can be neglected [23] due to the high buffering capacity inside the lumen [43]. According to this hypothesis (tested in section 2), ECS changes which are strictly speaking proportional to $\Delta\Delta\Psi$, equally reflect changes in the electrochemical proton gradient ($\Delta\Delta\tilde{\mu}_{H^+}$).

Fig 1A illustrates how the baseline $\Delta\tilde{\mu}_{H^+\,dark}$ prior to the pulse influences the amplitude and kinetics of the pulse-induced ECS (or $\Delta\Delta\tilde{\mu}_{H^+}$). To do so, we analyzed in water-infiltrated leaves at high and low [ATP]/([ADP][P]) ratios, respectively. Low [ATP]/([ADP][P]) ratios were obtained when respiratory ATP production was hampered in dark-adapted leaves by application of the cytochrome bc_1 inhibitor antimycin-A (AA, open symbols in Fig 1). AA addition exploits the genetically regulated nucleotide import machinery which metabolically couples chloroplast ATP levels to mitochondrial respiration [23, 32, 44-47]. On the contrary, high [ATP]/([ADP][P]) ratios were reached after building up ATP following a 30-s illumination (closed symbols). In all curves of Fig 1A, the ECS reached a plateau during the pulse which was followed by a fast decay phase in darkness. Both amplitudes of the plateau level and the fast decay phase depend on the light intensity of the applied pulse (Fig S3, not varied in the main text). The fast phase likely involves H^+ leaks above a critical $\Delta\tilde{\mu}_{H^+}$ ($\Delta\tilde{\mu}_{H^+\,leak}$), which is an *absolute* $\Delta\tilde{\mu}_{H^+}$ reference in a given material *in vivo* [23]. This fast phase finishes after 10 ms when the ECS decay kinetics becomes independent of the pulse light intensity (Fig S3), reflecting ATP synthesis [23]. The 10-ms ECS signal in darkness ($\Delta\Psi_{10ms}$) is therefore independent of pulse intensity,

and also independent of the physiological conditions preceding the pulse. Thus, the $\Delta\Psi_{10ms}$ will be used hereafter as the *experimental* reference of $\Delta\tilde{\mu}_{H^+}$. In turn, the ECS data in the following will be expressed as negative values ($\Delta\Psi - \Delta\Psi_{10ms}$; Fig 1B) which corresponds to the "remaining empty volume" of the opaque bottle analogy. Considering the outlined method, the larger pulse-induced ECS amplitude in the presence of AA than after the pre-illumination is related to a lower basal $\Delta\tilde{\mu}_{H^+dark}$ before the pulse in AA samples (Fig 1A). This was revealed after rescaling to our *experimental* reference $\Delta\Psi_{10ms}$ (-6.7 vs. >-3.5 charge separations/PSI, Fig 1B). After the 30-s illumination and the following re-adaptation to darkness, the increase of the pulse amplitude with the time in darkness (Fig 1A), again, indicated the continuous decrease of the $\Delta\tilde{\mu}_{H^+dark}$ (Fig 1B) and reflected the consumption of the extra ATP produced during the 30-s illumination.

According to Fig 1B and a previous report [23], the ECS decay kinetics after the pulse displayed three phases. The first phase, completed in 10 ms and discussed before, was systematically discarded. A second phase was completed in ~100 ms (phase 2) and was linked to ATP synthesis. Then, a multiphasic slow decay (phase 3, completed in ~1 min) was observed only once the $\Delta\tilde{\mu}_{H^+}$ fell below a threshold (at the end of phase 2, ~100 ms). This threshold corresponds to the $\Delta\tilde{\mu}_{H^+activation}$ described before [17, 19-23] and represented a second reference level, about 2 charge separations/PSI below $\Delta\Psi_{10ms}$ (arrowhead in Fig 1B). Phase 3 indicated a slowly active CF_1F_o, or, alternatively, a small CF_1F_o fraction staying fully active.

We first decided to check whether this quantitative measurement of the $\Delta\tilde{\mu}_{H^+dark}$ remained valid regardless of the redox regulation mechanism. Figs 1C and 1D show similar experiments on WT leaves infiltrated with the thiol reductant TCEP to cleave the γ-disulfide. Furthermore, the samples were in the same physiological conditions as in Figs 1A and 1B (AA-treated or pre-illuminated samples). In all cases, the ECS generation and the decay in the first tens of ms after the end of the pulse resembled the untreated sample (Fig 1C). As in water-infiltrated leaves, AA-treated leaves in the presence of TCEP showed a lower $\Delta\tilde{\mu}_{H^+dark}$ and illumination increased this pedestal (dashed lines in Fig 1D), reflecting ATP accumulation during pre-illumination and consumption during re-adaptation to darkness. The $\Delta\tilde{\mu}_{H^+}$ decay kinetics always seemed monophasic; we did not observe the slow phase of ECS decay (absence of phase 3 in Fig 1D). This was true even in conditions where $\Delta\tilde{\mu}_{H^+dark}$ was below the $\Delta\tilde{\mu}_{H^+activation}$ of Fig 1B, i.e., when dark re-adaptation after the 30-s illumination was longer than 9 min or in AA-treated samples. This observation at low $\Delta\tilde{\mu}_{H^+}$ was in agreement with the higher CF_1F_o activity measured *in vitro* upon cleaving the γ-disulfide by chemical thiol reductants [36]. A quantitative analysis will be given in section 4, demonstrating how the effect of the γ-redox state influences the $\Delta\tilde{\mu}_{H^+}$ dependence of CF_1F_o activity. The comparison of the control and TCEP-treated leaves validate our first hypothesis (mentioned in the introduction): The proposed protocol to measure the $\Delta\tilde{\mu}_{H^+dark}$ works in both the reduced and oxidized state, provided that no ΔpH is generated during the pulse. This absence of pulse-induced ΔpH corresponds to the second hypothesis, which will be addressed in the next section.

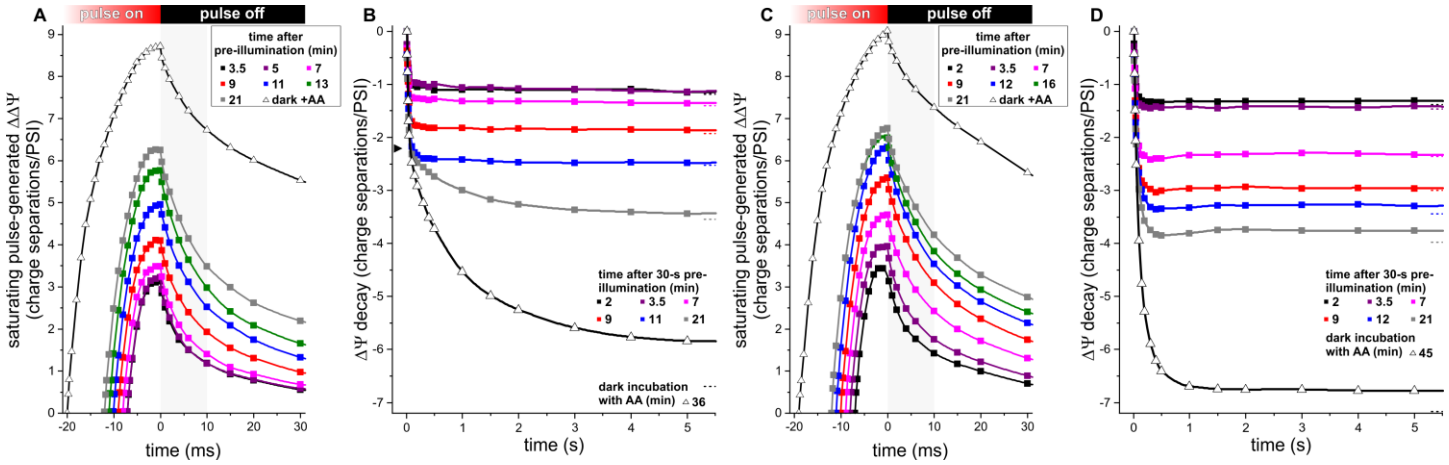

Fig 1: Pulse-induced ECS kinetics are shown in water-infiltrated leaves in the absence (A-B) or presence (C-D) of the mild reductant TCEP at 50 mM. Dark-adapted leaves were illuminated for 30 s (green-orange LED, 1000 µmol photons m^{-2} s^{-1}), followed by a dark re-adaptation for several minutes (indicated in the legend). +AA: infiltrated with 40 µM antimycin-A without illumination. All the measurements were made on different leaves from the same plant. In panels A and C, the dark-adapted (baseline) ECS level was arbitrarily set to 0 and only the ECS kinetics during the pulse and in the initial relaxation phases are shown. In panels B and D, the $\Delta\Psi_{10ms}$ values of all curves were set to 0 and only the ECS relaxation in the dark is shown (the value reached after 1 min relaxation is indicated with three dots on the right). The rapid transition between the fast and slow relaxation phases ($\Delta\tilde{\mu}_{H^+\text{activation}}$) is indicated in panel B by an arrowhead. The homothetic ECS curves in TCEP samples of panel D decayed without an apparent $\Delta\tilde{\mu}_{H^+\text{activation}}$, and the major decay finished within ~1-s.

2. *Obtaining the relative extent of $\Delta\Psi$ and ΔpH induced by short light pulses.*

For the interpretation of the previous results regarding the evolution of $\Delta\tilde{\mu}_{H^+}$, we followed the opaque bottle analogy and have made the hypothesis that the $\Delta\Psi_{10ms}$ reference served as our $\Delta\tilde{\mu}_{H^+}$ reference. This implied that the ΔpH generated until reaching $\Delta\Psi_{10ms}$ was insignificant, and only $\Delta\Psi$ increased during the short saturating light pulses. The demonstration of a negligible ΔpH contribution is crucial for this ECS-based method before introducing $\Delta\tilde{\mu}_{H^+}$-dependent CF_1F_o activity profiles in section 4, focusing on thiol modulation.

To test our hypothesis, we applied saturating light pulses of variable duration to dark-adapted leaves and probed the extra $\Delta\Psi$ ($\Delta\Delta\Psi$), extra ΔpH ($\Delta\Delta$pH) and their sum ($\Delta\Delta\tilde{\mu}_{H^+}$) remaining after a relatively short (15 s) dark recovery. To obtain those values, we applied a short 12-ms probing pulse 15 s after the first one and compared to a similar 12-ms probing pulse applied on a non-perturbed sample (dark line and symbols, Fig 2A). The $\Delta\Psi$ was monitored throughout the measurement and $\Delta\Delta\Psi$ was calculated as the difference between the dark-adapted ECS signal before the first light perturbation and the ECS signal 15 s later (Fig 2A). The $\Delta\Delta$pH after 15 s was derived from the 12-ms probing pulse, i.e., from the difference of its $\Delta\Psi_{10ms}$ value compared to fully dark adapted leaves (Fig 2A). A $\Delta\Delta$pH usually appeared after prolonged light pulses but this was not the case in Fig 2A. Therein, the ionophore nigericin (Nig) was used to exchange H^+ with K^+ as a proof of principle to favor $\Delta\Delta\Psi$ at the expense of $\Delta\Delta$pH. It is important to note that Nig also collapsed the proton motive force for mitochondrial ATP synthesis and thus interfered with metabolic coupling between the organelles. Accordingly, Nig infiltration resulted in a collapse of $\Delta\tilde{\mu}_{H^+\text{dark}}$ in the chloroplast (within ~15-30 min

incubation, see Fig S4 and Supplementary discussion). A duration of 15 s dark was necessary in this experiment to allow a partial relaxation of the electron carriers toward the dark-adapted state. Indeed, at the end of the first light pulse, the photochemistry of both photosystems was low due to the absence of acceptors (oxidized plastoquinones or oxidized ferredoxins) or donors (reduced P700). If the second light pulse was applied too early, photochemistry was insufficient to reach the $\Delta\tilde{\mu}_{H^+leak}$ which made measurement of the $\Delta\tilde{\mu}_{H^+}$ impossible.

We followed those parameters in water-infiltrated (Fig 2B) and in Nig-treated leaves (Fig 2C) for different durations of the first pulse (10 ms to 1 s light perturbation). Regardless of the first pulse duration, in both treatments the $\Delta\Psi_{10ms}$ upon the second pulse was smaller than in the corresponding dark-adapted sample. This indicated that a significant amount of extra ATP, generated during and after the first illumination, was still present after 15 s dark and increased the ΔpH ($\Delta\Delta$pH) compared to the dark-adapted level. The ionophore Nig attenuated $\Delta\Delta$pH (Fig 2C) but in water-infiltrated samples (Fig 2B), the $\Delta\Delta$pH increment was significant only between the 100-ms and 500-ms light perturbations. These samples also sustained a significant $\Delta\Delta\Psi$, up to 0.4 charge separation/PSI (dashed line in Fig 2B), although a stagnation for pulses longer than 100-ms was observed. The $\Delta\Delta\Psi$ after 15 s was always higher than 1 charge separation/PSI when Nig was present, even for the shortest durations of the light pulse (dashed line in Fig 2C). The lowered $\Delta\tilde{\mu}_{H^+dark}$ by the drug also influenced the $\Delta\Delta\tilde{\mu}_{H^+}$ 15 s after a 10-ms pulse, increasing it from 0.2 in controls (Fig 2D) to 1.4 charge separations/PSI in Nig samples (Fig 2E). For a 1-s pulse, those values reached 1.1 and 2.8 charge separations/PSI for control and Nig samples, respectively.

The fact that short pulses (below 100 ms, Fig 2D) generated only small changes in ΔpH (smaller than 0.1 charge separation/PSI) validated our initial hypothesis. This indicated that, if probing light pulses remain short, the ECS pulse method allowed the quantitative measurement of $\Delta\tilde{\mu}_{H^+}$ with a potential error of 0.1 charge separation/PSI only. The higher $\Delta\tilde{\mu}_{H^+}$ storage after 15 s dark in the Nig samples was simply due to the slower relaxation of the pulse-induced $\Delta\tilde{\mu}_{H^+}$ when the $\Delta\tilde{\mu}_{H^+dark}$ was far below the $\Delta\tilde{\mu}_{H^+activation}$, as we described before in the case of the AA treated sample (Fig 1B). The uncoupling by Nig was more efficient in collapsing $\Delta\tilde{\mu}_{H^+dark}$ compared to AA but, like other uncouplers, Nig modified the different phases of ECS decay kinetics (Fig S4, see also Supplementary discussion). Therefore, membrane integrity-preserving AA will be preferred for unbiased CF_1F_o analysis at low $\Delta\tilde{\mu}_{H^+dark}$ (section 4).

In the first two sections, we have shown that our methodology is valid regardless of the redox state of CF_1F_o. Moreover, it allows quantitative measurements of the $\Delta\tilde{\mu}_{H^+dark}$ (relative to the $\Delta\tilde{\mu}_{H^+}$ reference given by $\Delta\Psi_{10ms}$) provided that the saturating light pulse is (i) strong enough to reach the $\Delta\tilde{\mu}_{H^+leak}$ (which is valid for the 2000 photons/PSI/s light irradiance used here), and (ii) short enough to avoid the generation of ΔpH (which is valid for pulses shorter than 100 ms). This allows to follow the kinetics of the $\Delta\tilde{\mu}_{H^+dark}$ after a light perturbation in the next part.

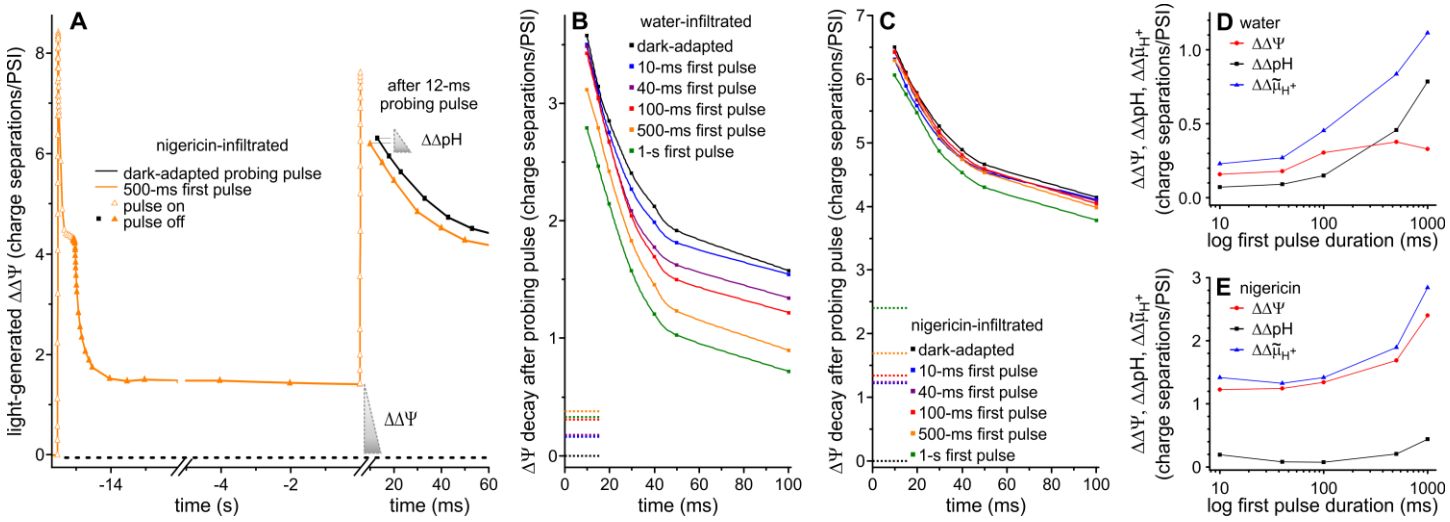

Fig 2: The estimation of $\Delta\Delta\Psi$, $\Delta\Delta$pH and $\Delta\Delta\tilde{\mu}_{H^+}$ generated by an illumination is shown. The parameters were measured 15 s after a saturating pulse of various duration. (A) Exemplary ECS measurement in the presence of nigericin (open symbols light on, closed symbols darkness) measured as the difference between the absorption changes at 520 nm and the one at 546 nm (see Methods). The leaf was illuminated with a first pulse of 500-ms (t ~ -15 s), then ECS was followed for 15 s in the dark and a 12-ms probing pulse was used to determine the new $\Delta\Psi_{10ms}$ reference (the probing pulse ended at t = 0 s). For the sake of visualization, the dark-adapted ECS decay was shifted on the x-axis by 3 ms. (B) and (C) The initial phase of the $\Delta\Psi$ decay after the 12-ms pulse is shown for leaves infiltrated with (B) water and (C) nigericin. The $\Delta\Delta\Psi$ at the end of the 15-s dark period is indicated by horizontal dashed lines. The $\Delta\Delta$pH corresponds to the difference between the $\Delta\Psi_{10ms}$ after the saturating pulse and the one of a dark-adapted leaf (black closed squares). (D) and (E) The relationship of $\Delta\Delta\Psi$, $\Delta\Delta$pH and $\Delta\Delta\tilde{\mu}_{H^+}$ with the duration of the first light pulse are shown for (D) water and (E) nigericin infiltrated leaves. All the measurements in this figure were performed with leaves from the same plant, and are the representative outcome of two independent experiments.

3. Showing that the sustained $\Delta\tilde{\mu}_{H^+dark}$ elevation is a function of extra ATP after an illumination.

In this section, we use the method to follow the fate of the $\Delta\tilde{\mu}_{H^+}$ after an illumination by supposing that the thermodynamic equilibrium is met during a dark period before the ECS measurement, and that following $\Delta\tilde{\mu}_{H^+}$ is equivalent to following the [ATP]/([ADP][P]) ratio.

After the 30-s illumination in water-infiltrated leaves (Fig 1B and additional measurements from the same experiment), we re-plotted the $\Delta\tilde{\mu}_{H^+dark}$ values as a function of the time in darkness (Fig 3A, black open squares). The $\Delta\tilde{\mu}_{H^+dark}$ after the 30-s illumination was ~-1.2 charge separations/PSI relative to the $\Delta\tilde{\mu}_{H^+}$ reference ($\Delta\Psi_{10ms}$) in the water-infiltrated leaf (black open squares in Fig 3A); being significantly higher than in the dark-adapted sample (~-4 charge separations/PSI, black dashed line). After ATP formation in the light, the elevated $\Delta\tilde{\mu}_{H^+dark}$ remained constant for 5 min and, due to slow ATP consumption [23], relaxed towards the dark-adapted value in ~30 min (Fig 3A). When leaves were infiltrated with Nig before the 30 s illumination (open triangles in Fig 3A), the $\Delta\tilde{\mu}_{H^+dark}$ reached a lower level (-2.3 charge separations/PSI after 2 min dark) and relaxed to an even lower value within ~15 min (-6.3 charge separations/PSI). As discussed, Nig may interfere with mitochondrial ATP production in darkness, resulting in a lower $\Delta\tilde{\mu}_{H^+dark}$ and more rapid depletion of extra ATP upon illumination.

The closed symbols in Fig 3A also show the lifetime of $\Delta\tilde{\mu}_{H^+dark}$ and ATP in non-infiltrated WT leaves after illuminations of different durations (between 3-s and 12-min). Interestingly, the elevated $\Delta\tilde{\mu}_{H^+dark}$ became independent on the illumination duration beyond 7 s (between ~-1.3 to -1.5 charge separations/PSI). Moreover, a lag was observed in the relaxation, which increased with the time of illumination. Once ATP levels decreased slowly over ~20 min, the $\Delta\tilde{\mu}_{H^+dark}$ reached a stable dark level which corresponded to the dark-adapted value (~-3.5 charge separations/PSI, black solid line). The water infiltration treatment had no effect, at least for illuminations not longer than 30 s, since the curve for infiltrated leaves illuminated for 30 s was in between the 15-s and 40-s illumination curves of the non-infiltrated ones (Fig 3A). To conclude, the $\Delta\tilde{\mu}_{H^+dark}$ is dependent on the physiological conditions. Nucleotide exchange between cell compartments is strictly controlled and, compared to the reversible CF_1F_o, passive ion movements across the membrane are slow [23, 32, 44-47].

We also analyzed the light-induced changes of $\Delta\tilde{\mu}_{H^+dark}$ in the reduced and oxidized CF_1F_o forms before establishing a specific $\Delta\tilde{\mu}_{H^+}$ dependency of CF_1F_o activity (next section). Besides infiltrating leaves with the thiol reductant TCEP, we also looked at the behavior of the *gamera* mutant, in which the CF_1F_o is in its reduced isoform (γ-dithiol) in the dark [28]. The $\Delta\tilde{\mu}_{H^+}$ threshold ($\Delta\tilde{\mu}_{H^+activation}$) at ~100 ms in darkness is characteristic for water-infiltrated samples with the γ-disulfide (arrowhead in Fig 3B, see also Fig 1B). It disappeared in presence of TCEP due to accelerated $\Delta\tilde{\mu}_{H^+}$ decay kinetics at the end of phase 2. The $\Delta\tilde{\mu}_{H^+}$ decay kinetics was even more accelerated in the *gamera* mutant. This phenotype, obtained in the *dpa1* genetic background [28], could be unambiguously attributed to the dithiol since the behavior of the *ATPC1*-complemented *dpa1* mutant, *dpa1c*, was similar to the WT (Fig 3B; ATPC1 is the thioredoxin-sensitive γ-subunit isoform and ATPC2 is the isoform present in *gamera*). Based on the pronounced slowdown of the $\Delta\tilde{\mu}_{H^+}$ decay after phase 2, we conclude that CF_1F_o was present mainly in its oxidized state in dark-adapted WT leaves, in contradiction with a previous report [23]. Incomplete γ-disulfide reduction by TCEP infiltration resulted in a mixture of active and inactive CF_1F_o (distributed homogeneously along the thylakoid membrane) and a continuous decay kinetics of the $\Delta\tilde{\mu}_{H^+}$.

In TCEP-treated leaves, the $\Delta\tilde{\mu}_{H^+dark}$ attained after the 30-s illumination was similar to the one in water-infiltrated leaves (~-1.5 charge separations/PSI, blue open squares in Fig 3A). The capacity to

sustain an elevated $\Delta\tilde{\mu}_{H^+dark}$ after illumination was slightly less pronounced in TCEP samples. We cannot rule out that TCEP infiltration also influenced the metabolic ATP sink capacity in the dark or produced mild uncoupling of the membranes. We tested whether the effect of TCEP on thiol modulation developed further during the illumination and following relaxation in the dark, and concluded that this effect is stable throughout the experiment (Fig S6). It is noteworthy that, at variance with the effect of commonly used dithiothreitol (DTT), the kinetics of the fluorescence increase in a dark-adapted leaf was not altered upon TCEP infiltration, eliminating a potential side effect on the plastoquinone pool redox state (not shown). In a similar experiment, we analyzed the effect of a 14-min pre-illumination on a non-infiltrated *gamera* mutant leaf (closed circle in Fig 3A). At variance with the results obtained in the WT, we observed that illumination of the *gamera* mutant induced a decrease of the $\Delta\tilde{\mu}_{H^+dark}$ that returned to the dark-adapted level very slowly in ~ 45 min (see red horizontal line). We conclude that ATPC2 produced a perturbation of CF_1F_o that prevented long term ATP accumulation during illumination. A lower *gamera* proton conductivity in steady-state light was reported [28] which might reflect this CF_1F_o perturbation. The latter could be related to the large slowdown of Calvin-Benson cycle activation (about a factor 4) and the larger transient NPQ formation observed on the mutant with respect to the WT (see Fig S5). This section demonstrates that the ECS-based $\Delta\tilde{\mu}_{H^+dark}$ estimations provide thermodynamic snapshots of the [ATP]/([ADP][P]) ratio in the chloroplast.

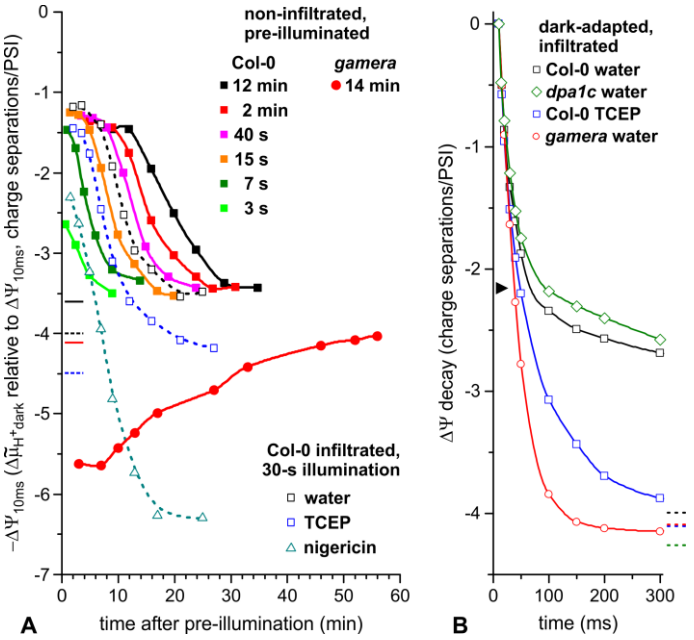

Fig 3: Light-induced ATP lifetime measurements and membrane potential ($\Delta\Psi$) decay kinetics in various Arabidopsis genotypes are shown. (A) The effect of the γ-disulfide bond reduction on ATP accumulation and relaxation after an illumination of different durations is displayed. The $\Delta\tilde{\mu}_{H^+dark}$ values are relative to the $\Delta\Psi_{10ms}$ and horizontal lines refer to fully dark-adapted, non-infiltrated (solid) and infiltrated (dashed) samples. The water-/TCEP-infiltrated WT samples were from the same plant, and the varied pre-illumination experiments were performed on another plant. (B) Initial $\Delta\Psi$ decay kinetics of the WT are shown (infiltrated in the dark with water or 50 mM TCEP), as well as the *gamera* mutant and the *ATPC1*-complemented *dpa1* mutant, termed *dpa1c*. The slowdown at ~100 ms is shown with an arrowhead. Dashed lines indicate the $\Delta\Psi$ decay value 1 min after the pulse.

4. *Obtaining $\Delta\tilde{\mu}_{H^+}$-dependent CF_1F_o activity profiles in the two γ-subunit redox states.*

The final aim of this work is to determine how the reduction/oxidation of the γ-disulfide modifies the $\Delta\tilde{\mu}_{H^+}$ regulation of CF_1F_o activity. As outlined above, the pulse-induced ECS method to measure $\Delta\tilde{\mu}_{H^+}$ has been established and validated in both redox states. For CF_1F_o activity determination, the ECS decay rate after a single turnover laser flash is routinely obtained from exponential decay functions [e.g., Ref. 42]. However, there is a bias due to the "*b* phase": a ~10-ms ECS rise after the flash due to electrogenic contribution of the cytochrome b_6f activity which superimposes on the CF_1F_o-related ECS decay. Moreover, we observed another poorly understood but precedingly documented [16, 17] source of variation when using flashes. In short, the ECS decay rate after a flash not only depends on the $\Delta\tilde{\mu}_{H^+dark}$ but also on whether the $\Delta\tilde{\mu}_{H^+activation}$ was surpassed during the light perturbation. We tried to circumvent these sources of error and mitigate their contributions to the ECS decay by surpassing $\Delta\tilde{\mu}_{H^+activation}$ in all of our measurements, thus producing $\Delta\tilde{\mu}_{H^+}$-activated CF_1F_o (by 8-ms to 17-ms saturating pulses depending on the $\Delta\tilde{\mu}_{H^+dark}$; see Fig 4). We then measured the rate constant of CF_1F_o as the slope of the ECS decay when ECS signals reached the level expected after a saturating laser flash (i.e., $\Delta\tilde{\mu}_{H^+dark}$ +1 charge separation/PSI; see Fig 4). This procedure offered another advantage: At the time of the slope measurement, i.e., few tens or hundreds of ms after the end of

the pulse, the contribution of the *b* phase was negligible compared to CF_1F_o activity, although b_6f-catalyzed electron transfer between $P700^+$ and PQH_2 lasted longer in our measurements.

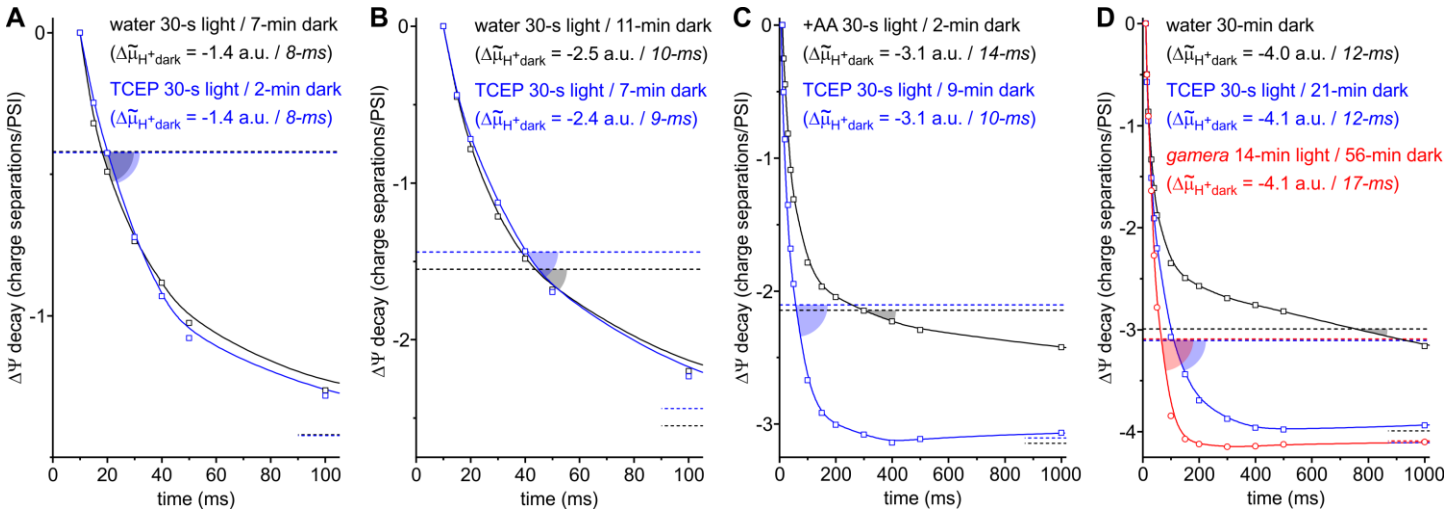

Fig 4: Calculation of the CF_1F_o rate from the ECS decay kinetics is shown in water- and TCEP-infiltrated WT, as well as *gamera* (only in panel D since the mutant could not accumulate ATP in the light and therefore sustained a lower $\Delta\tilde{\mu}_{H^+dark}$). The data is part of Fig 5A and the rationale was to calculate the CF_1F_o rate when the electrochemical proton gradient reached $\Delta\tilde{\mu}_{H^+dark}$ +1, in relation to the classical single turnover flash ECS decay protocol. Each panel compares samples with similar $\Delta\tilde{\mu}_{H^+dark}$ (-1.4, -2.5, -3.1 and -4 charge separations/PSI) from Figs 1B, 1D and 3B. The dashed lines on the bottom right indicate the $\Delta\tilde{\mu}_{H^+dark}$ and the upper dashed lines represent $\Delta\tilde{\mu}_{H^+dark}$ +1 charge separation/PSI. The semi-transparent angles visualize the ECS decay rate at this point, expressed as *R* in Fig 5A. The $\Delta\tilde{\mu}_{H^+dark}$ was estimated by a ms-pulse and its duration is given in italics. In panels A and B, the $\Delta\tilde{\mu}_{H^+dark}$ remained above the $\Delta\tilde{\mu}_{H^+activation}$ and only a fast phase of ECS decay was seen in both γ-redox states. In panels C and D, the $\Delta\tilde{\mu}_{H^+dark}$ was below the $\Delta\tilde{\mu}_{H^+activation}$ of water-infiltrated WT leaves and the ECS decay kinetics became biphasic in these samples. In the latter, the break in the $\Delta\tilde{\mu}_{H^+}$ decay kinetics at the end of phase 2 revealed a CF_1F_o transition from an active toward an inactive form.

Fig 5A sums up all the CF_1F_o rate constants (obtained at $\Delta\tilde{\mu}_{H^+dark}$ + 1 charge separation/PSI) as a function of the corresponding $\Delta\tilde{\mu}_{H^+}$ values. The data presented in this manuscript so far lays the foundations for Fig 5A: WT leaves (dark-adapted or during relaxation following a 30-s illumination), TCEP-treated WT leaves in the same conditions, as well as *gamera* leaves (dark-adapted or following a 14-min illumination). Fig 5A also contains additional measurements obtained in comparable experiments, such as dark-adapted *gamera* leaves in the presence of AA. The CF_1F_o activity vs. $\Delta\tilde{\mu}_{H^+}$ curves of the reduced (*gamera* isoform) and oxidized (water-infiltrated WT) enzyme resembled the ones obtained *in vitro* [36]. The TCEP-infiltrated WT was intermediate, in agreement with a mixed CF_1F_o redox population. Fig 5A shows that below $\Delta\tilde{\mu}_{H^+activation}$ of the oxidized form (~-2.2 charge separations/PSI, see arrowhead in Fig 1B, Fig 3B), the CF_1F_o was always faster in the (partially) reduced form. The rate constant of CF_1F_o increased exponentially with $\Delta\tilde{\mu}_{H^+}$ in the reduced form, as soon as $\Delta\tilde{\mu}_{H^+}$ was above ~-4.7 charge separations/PSI (Fig 5A).

Both $\Delta\tilde{\mu}_{H^+}$-dependent activities of (chemically unmodified) CF_1F_o in WT and *gamera* have been fitted with a sigmoid function, similar to the *in vitro* study in spinach using thiol agents [36]. In fact, the plotted CF_1F_o rate constants of both genotypes were processed in one calculation by using a sum of

two sigmoid functions (Fig 5A). In Equation 1, we forced via the constant *c* the first summand to be zero in the *gamera* plot, and the second summand to be zero in the WT plot:

$$y = c \times \left(\frac{A1}{1 + 10^{(x0.ox - x) \times p}}\right) + (1 - c) \times \left(\frac{A1}{1 + 10^{(x0.red - x) \times p}}\right) \quad \text{(Eq.1).}$$

A1 defines shared maximal rate constants of 41.4 ± 2.8 s^{-1} (± standard error). The slope parameter of the function is expressed as *p* (0.9 ± 0.1). The $\Delta\tilde{\mu}_{H^+}$ where the half-maximal CF_1F_o activities were obtained for WT and *gamera* are defined as *x*0.*ox* (-1.0 ± 0.1 charge separations/PSI) and *x*0.*red* (-3.6 ± 0.1 charge separations/PSI), respectively. The TCEP sigmoid fitting curve in Fig 5A was obtained with *c* = 0.54 ± 0.04, suggesting about 54% of CF_1F_o in the oxidized γ-disulfide conformation. Incomplete γ-disulfide cleavage could be related to the limited efficiency of TCEP [48]. This efficiency value was close to the fraction of reduced CF_1F_o in the presence of TCEP in Fig 5B, estimated from the ECS decay kinetics in *gamera* and WT (already presented in Fig 3B). In Fig 5B, the relaxation of ECS from the $\Delta\tilde{\mu}_{H^+\text{activation}}$ (arrowhead) to $\Delta\tilde{\mu}_{H^+\text{dark}}$ (~-4 charge separation/PSI for the 3 curves) was fitted with a mono-exponential decay. Rate constants of 0.8 s^{-1} in water-infiltrated WT were obtained in the presence of ~100% γ-disulfide, and 30.6 s^{-1} were measured with 100% γ-dithiol in *gamera*. Accordingly, Fig 5B suggests that TCEP infiltration produced ~58% γ-disulfide cleavage in WT CF_1F_o since the rate constant was 13.4 s^{-1}. Unexpectedly, the partially reduced TCEP samples in Fig 5A showed a faster ECS decay at the low $\Delta\tilde{\mu}_{H^+\text{dark}}$ +1 charge separation/PSI when AA was present (an ECS decay kinetics comparison with fully reduced *gamera* CF_1F_o is shown in Fig S7).

Supporting previous reports [36, 49], we did not observe an effect of the redox regulation on the maximal CF_1F_o activity at high $\Delta\tilde{\mu}_{H^+}$ in WT. However, we did not manage to sustain high enough $\Delta\tilde{\mu}_{H^+\text{dark}}$ to fully describe the plateau of maximal CF_1F_o activities (see 95% confidence intervals in Fig 5A). This was due to experimental constraints: First, in the oxidized form, it was not possible to reach higher values of $\Delta\tilde{\mu}_{H^+}$ because a sufficient dark period was needed after the 30 s illumination to reoxidize PSI and PSII acceptors. Second, illumination decreased the $\Delta\tilde{\mu}_{H^+}$ in the reduced *gamera* CF_1F_o (Fig 3A). Still, the observation that half-reduced TCEP samples and oxidized WT leaves produced similar rate constants at $\Delta\tilde{\mu}_{H^+}$ ~-0.5 charge separation/PSI suggests that the CF_1F_o activities in both redox states were similar in this range of $\Delta\tilde{\mu}_{H^+}$ (Fig 4A, Fig 5A).

Taken together, this section demonstrates that the CF_1F_o redox state has a significant impact on its enzymatic activity *in vivo* and confirms previous *in vitro* studies: The reduced form of CF_1F_o (in the *gamera* mutant, but also partially in the TCEP-treated WT) exhibited higher activity at low membrane energization.

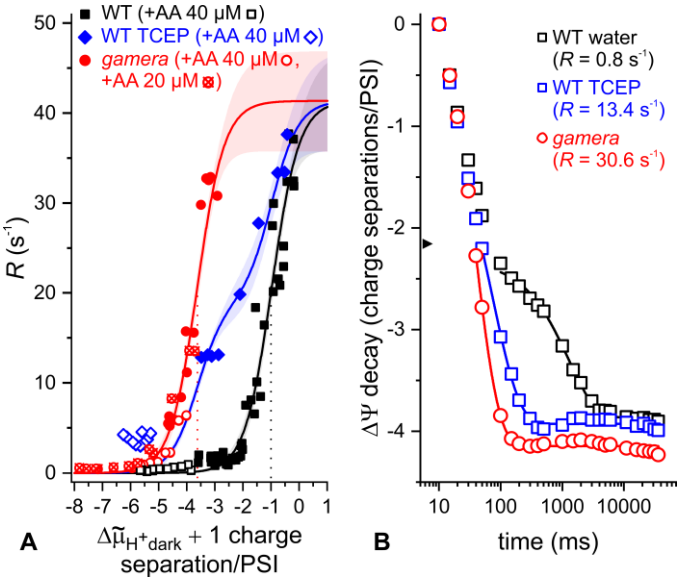

Fig 5: The regulation levels of $\Delta\tilde{\mu}_{H^+}$ and thiol modulation on ATP synthesis are shown. (A) The $\Delta\tilde{\mu}_{H^+}$-dependence of the CF_1F_o activity in the oxidized (black) and reduced (red) forms are shown, as well as in the intermediate situation of TCEP-infiltrated WT leaves (blue). Closed symbols: untreated leaves, open symbols: leaves were additionally infiltrated with 40 µM and 20 µM antimycin-A (+AA). The $\Delta\tilde{\mu}_{H^+}$ in each color-coded group was modulated in independent samples (*n* in closed/open black 3/2, blue 1/2, red 1/3). Decay rate constants, *R*, were obtained according to Fig 4. Fitted curves were calculated with Equation 1 and the 95% confidence intervals are transparent. The water-infiltrated WT showed a $\Delta\tilde{\mu}_{H^+\text{activation}}$ of ~-2.2 charge separations/PSI, and half-maximal *R* at ~-1.0 charge separations/PSI (dotted black line). The γ-dithiol-containing *gamera* showed a half-maximal *R* at ~-3.6 charge separations/PSI (dotted red line) and a $\Delta\tilde{\mu}_{H^+\text{activation}}$ of ~-4.7 charge separations/PSI. (B) Different kinetics of the ECS decay are shown in the control and TCEP-treated WT, as well as the *gamera* mutant at similar $\Delta\tilde{\mu}_{H^+\text{dark}}$. Indicated by fitted ECS relaxation curves, a mono-exponential decay function starting below $\Delta\tilde{\mu}_{H^+\text{activation}}$ of the WT water sample (arrowhead) was used to calculate *R* of the CF_1F_o.

Discussion

Before finally visualizing the changing CF_1F_o activity *in vivo* (Results section 4), various methodical requirement were met to refine the ECS protocol [23] that estimates the $\Delta\tilde{\mu}_{H^+dark}$. To do so, we presented in section 2 that short saturating pulses do not generate a ΔpH and that pulse-induced ECS changes reflect changes in $\Delta\tilde{\mu}_{H^+}$. In section 3, we showed that the measured $\Delta\tilde{\mu}_{H^+dark}$ is a metabolic feature, defined by the [ATP]/([ADP][Pi]) ratio at thermodynamic equilibrium, and that leak processes are negligible. The final CF_1F_o characterization let us conclude that the WT enzyme is in an oxidized state in the dark, contrary to a previous report [23]. The rate constants we measured in the low $\Delta\tilde{\mu}_{H^+}$ range (Fig 5A) were not zero although it was previously proposed that the CF_1F_o was fully inactive below the $\Delta\tilde{\mu}_{H^+activation}$ [16, 17]. If so, the activities below the apparent $\Delta\tilde{\mu}_{H^+activation}$ in Fig 5B (0.8 s^{-1} in WT vs. 30.6 s^{-1} in *gamera*) would mean that 2-3% of the CF_1F_o was in the reduced form in the dark-adapted state *in vivo*, matching *in vitro* findings [49].

In the following four sections, we will discuss (i) the caveats of the presented CF_1F_o data for strict comparisons with the *in vitro* results, (ii) the sustained impact of an illumination period on $\Delta\tilde{\mu}_{H^+dark}$, (iii) possible side effects of chemical infiltration with TCEP, and (iv) structure-function considerations.

(i) Precautions for strict comparisons of the presented CF_1F_o data with in vitro results.

Overall, the obtained CF_1F_o rate versus $\Delta\tilde{\mu}_{H^+}$ curves *in vivo* resembled earlier *in vitro* results in spinach chloroplasts where maximal ATP synthesis activity was independent from the redox state, while half-maximal rates of reduced CF_1F_o occurred at a lower ΔpH of ~0.7 units [36]. This corresponds to a difference of ~42 mV when expressed in $\Delta\Psi$ equivalent. In our results, half-saturation of CF_1F_o was 2.6 charge separations/PSI higher in the oxidized WT form compared to the *gamera* mutant. The *in vivo* and *in vitro* results are therefore roughly compatible by accepting a value of ~20 mV per PSI charge separation, which is the most accepted estimate [40, 50, 51].

However, our results are not suited for strictly comparing the absolute values of the electrochemical gradient needed to reach half-saturation. The $\Delta\tilde{\mu}_{H^+}$ values in our work are expressed in relative values (by comparison to $\Delta\Psi_{10ms}$), whereas absolute values are reported in the *in vitro* work of Junesch and Gräber. For a proper *in vitro* and *in vivo* comparison, our results should be expressed in absolute values, too, which requires to obtain a situation where $\Delta\tilde{\mu}_{H^+dark}$ is zero. Several studies [23, 47] worked with appropriate inhibitors to completely collapse the $\Delta\tilde{\mu}_{H^+dark}$, including ours. The $\Delta\tilde{\mu}_{H^+dark}$ is built at the expense of the ATP present in the plastid in dark-adapted leaves, which originates from mitochondrial ATP production as has been shown previously for algae [52], diatoms [47], and vascular plants [23]. Although antimycin-A (AA) inhibits the cytochrome bc_1 complex in the mitochondrial respiratory chain, it is known that the treatment does not eliminate this cellular ATP source completely [47]. In that regard, we identified more effective treatments in WT (Fig S4) but lowering $\Delta\tilde{\mu}_{H^+dark}$ by AA is preferred in our CF_1F_o characterization study despite individual differences between samples (Supplementary discussion). Most importantly, the $\Delta\tilde{\mu}_{H^+dark}$-collapsing efficiency of the chemical does not involve direct modification of the membrane and its electric permeability.

With this in mind, it is possible to discuss our results in the light of the 2.7 and 3.4 ΔpH units for half-saturation of the reduced and oxidized ATP synthesis rate *in vitro* (see reference 36 and Fig S8A). Let us focus on oxidized samples where half-maximal rates *in vitro* were measured at a $\Delta\tilde{\mu}_{H^+}$ equivalent to ~201 mV [36]. This value yields ~10 charge separations/PSI with an estimated 20 mV per reaction center turnover [40, 50, 51]. By referring to $\Delta\Psi_{10ms}$, our relative $\Delta\tilde{\mu}_{H^+}$ values indicated half-saturation of oxidized CF_1F_o at -1.0 charge separation/PSI. We obtained the lowest values of $\Delta\tilde{\mu}_{H^+dark}$

for AA-infiltrated *gamera* leaves in our ECS data set which equilibrated down to ~-8.8 charge separations/PSI (note that *x*-axis in Fig 5A is $\Delta\tilde{\mu}_{H^+dark}$ +1). We expect a residual $\Delta\tilde{\mu}_{H^+dark}$ when solely relying on the respiratory inhibitor AA (Supplementary discussion). When matching half-saturation in both systems, the remaining $\Delta\tilde{\mu}_{H^+dark}$ in our oxidized CF_1F_o data set should be ~2.2 charge separations/PSI (10 – 8.8 + 1.0), corresponding to ~44 mV or ~0.7 ΔpH units. Thus, we do acknowledge a significant discrepancy between our results and the ones obtained *in vitro* [36]. A tentative conversion of our relative oxidized CF_1F_o half-saturation values to an absolute $\Delta\tilde{\mu}_{H^+}$ expression yields 156 $\pm$ 22 mV ((8.8 – 1.0) $\times$ 20 mV; for reduced samples see also Fig S8B). We also consider the possibility that the $\Delta\tilde{\mu}_{H^+}$ at ATP synthesis half-saturation of the fully reduced ATPC1 γ-dithiol in WT leaves does not resemble CF_1F_o in *gamera* (see sections iii and iv).

(ii) What does the lifetime of ATP depend on?

In this work, we could measure the ATP lifetime after an illumination and showed that the accumulated ATP was saturated after 7 s of light. Prolonging the light duration only modified the lag before the ATP pool relaxed. We favor the hypotheses that the increased ATP lifetime, as a function of the pre-illumination period (closed squares in Fig 3A), was associated with the accumulation of high energy bonds in different plastid metabolites and/or that free ATP levels were buffered by the stromal adenylate kinase activity as proposed recently [53, 54]. The view that metabolic ATP consumption occurs within the chloroplast at higher rates than leaking towards other compartments is supported in a nucleotide transporter study. Therein, the ATP exchange rate between chloroplast and cytosol was rather slow, and free ATP diminished rapidly in the dark after illumination [32]. According to the fluorescent ATP sensor data, free MgATP levels varied in the stroma from 0.2 mM (darkness) to 0.5 mM (light), while cytosolic MgATP was about 2 mM [32, 55]. Thus, a delayed post-illumination decline of the $\Delta\tilde{\mu}_{H^+dark}$ in Fig 3A could be related to slow metabolite conversions that consume plastidic ATP. For instance, high levels of ribulose-1,5-bisphosphate and 1,3-bisphosphoglycerate in the Calvin-Benson cycle could be part of a feedback inhibition that prevents their own ATP-consuming synthesis. Furthermore, the deactivation of the Calvin-Benson cycle in the dark [23] was in the same time range as the decay of $\Delta\tilde{\mu}_{H^+dark}$. On the other hand, the thioredoxin targets fructose-1,6-bisphosphatase and sedoheptulose-1,7-bisphosphatase may have become partially reduced when infiltrating leaves with TCEP (midpoint redox potential of −290 mV [56]), thus favoring their activation. Additionally, it is not known whether TCEP influences the phosphate group transfer between ATP and AMP (yielding 2 ADP) through cysteine redox chemistry in chloroplast adenylate kinase 5 [53]. In turn, this could explain a slightly earlier onset of the consumption of ATP after 30-s illumination in TCEP-infiltrated samples (cf. open squares in Fig 3A).

(iii) Possible side effects of TCEP infiltration

In Fig 5A, the fit of the TCEP-infiltrated experimental data by the sum of two sigmoids failed at low $\Delta\tilde{\mu}_{H^+}$: significantly elevated rates were observed in the presence of TCEP + AA (open blue diamonds, see also Fig S7 for kinetics comparison with *gamera* + AA). We provide three possibilities for our observations, none of which we can endorse at this point: First, it is possible that γ-disulfide cleavage by TCEP was further advanced (>~50%) when the WT CF_1F_o population was under the influence of an increased cellular redox poise due to respiration inhibition. To further substantiate this hypothesis, the measurement of approximative $R < 1\ s^{-1}$ would have required the $\Delta\tilde{\mu}_{H^+dark}$ to collapse even below the values obtained in Fig 5A for TCEP + AA. The associated difficulties of achieving such situations are outlined in the Supplementary discussion. This hypothesis also implies that ATP synthesis onset in

reduced WT CF_1F_o is below that shown in Fig 5A for the *gamera* CF_1F_o isoform. Secondly, we cannot rule out that TCEP infiltration had weak uncoupling effects or, thirdly, modified ion channel/antiporter activity. Possible TCEP targets could be an activation of $\Delta\Psi$-consuming anion channels such as VCCN1 [2], or a deactivation of $\Delta\Psi$-generating H^+/cation antiporters such as KEA3 [1]. However, there is currently no evidence of VCCN1/KEA3 thiol regulation, nor were their activities analyzed at low $\Delta\tilde{\mu}_{H^+dark}$. It has been reported that reduction of chloroform-extracted CF_1 by DTT resulted in the reversible dissociation of the ε-subunit which would produce membrane uncoupling [57-59], if this was the case with TCEP *in vivo*. Accordingly, the slightly earlier onset of $\Delta\tilde{\mu}_{H^+dark}$ decrease upon illuminating TCEP-infiltrated samples might be due to a slow leak process (Fig 3A). Considering the remaining uncertainties on the TCEP + AA data, further studies are necessary to clarify whether CF_1F_o-independent processes produce slightly elevated ECS decay rate constants.

(iv) *Combining function, structure, and physiology*

In the following, we underpin our thiol modulation study in the light of structural findings since contribution of $\Delta\tilde{\mu}_{H^+}$ is poorly understood. The γ-redox domain as such forms an L-shaped double hairpin (Fig 6A, light green in magnified area). The second hairpin interacts with the β-subunit DELSEED motif and supposedly forms an ATPase chock during rotation in the oxidized state [34]. Alternatively, the γ-disulfide stabilizes the redox domain intrinsically rather than establishing the chock element [37]. Based on a proportion shift of the three rotary states, lower energetic barriers may occur during rotary transitioning due to an increased flexibility and lower torsional constraints in the reduced enzyme [37].

Critical structural alterations between the interactors (γ-redox domain and β-DELSEED loop) can be expected as a function of $\Delta\tilde{\mu}_{H^+}$. For instance, various buried residues (e.g., γK222 and βK399 in Fig 6A) have been chemically modified in illuminated thylakoids only [reviewed in 38, 60, 61]. Although details of these CF_1F_o rearrangements are not clear yet, the $\Delta\tilde{\mu}_{H^+}$ may transiently modify the sum of interactions with the β-DELSEED loops by uncovering parts of the γ-redox domain in a reversible fashion. In turn, the γ-redox domain exposure may enhance the chemical-to-mechanical energy transduction efficiency and could be a feature of the CF_1F_o activation. The influence of $\Delta\tilde{\mu}_{H^+}$ quantity [8] and quality [18] on CF_1F_o activation has been investigated by various groups.

Upon reaching $\Delta\tilde{\mu}_{H^+leak}$ in our experiments at the end of the ms-pulses, the $\Delta\tilde{\mu}_{H^+}$-activated CF_1F_o was obtained in both redox states (Fig 6B above dashed line). The surplus of $\Delta\tilde{\mu}_{H^+}$ was consumed at maximal rates during this ~100-ms phase in the dark until reaching a turning point, i.e., $\Delta\tilde{\mu}_{H^+activation}$ in WT (arrowhead in Fig 6B, the corresponding threshold in *gamera* was below the $\Delta\tilde{\mu}_{H^+dark}$). Stabilized by the disulfide, we hypothesize that the γ-redox domain is buried again which slows down the WT by altering the sum of interactions with the β-DELSEED loops (Fig 6B, below dashed line). It was shown that the redox domain experiences the $\Delta\tilde{\mu}_{H^+}$, becoming more solvent-accessible [25-27, 49, 62, 63]. The intrinsic $\Delta\tilde{\mu}_{H^+activation}$ in WT may represent the critical driving force level for ATP synthesis where transient resting times in between rotary states are long enough to allow for molecular relaxation during dwells. A different dwelling without the rigidity-enhancing γ-disulfide might account for a lower $\Delta\tilde{\mu}_{H^+activation}$ in *gamera*. Note that the amino acid sequences between ATPC1 (WT) and ATPC2 (*gamera*) are significantly different in the redox domain with profound effects on steady-state rates [64], which may relate to isoform-specific contacts with the β-DELSEED loop. Considering the effects and limits of chemical reduction (section iii), it is likely that disrupting the disulfide in ATPC1 by mutation will yield a different activity profile as shown in Fig 5A for *gamera*.

Conclusion

The intertwining of CF_1F_o and $\Delta\tilde{\mu}_{H^+}$ includes various regulatory loops such as thiol modulation which has physiological consequences. By increasing light utilization efficiency, a highly conductive CF_1F_o at low $\Delta\tilde{\mu}_{H^+}$ maximizes the photosynthetic output for CO_2 fixation. Here, we introduced and discussed a versatile spectroscopic *in vivo* assay to disentangle the molecular consequences of thiol modulation on the $\Delta\tilde{\mu}_{H^+}$ to ATP conversion efficiency. Moreover, the ECS protocol may be transferred to other CF_1F_o mutants in the future, for instance of the ε-subunit. Its C-terminus was found retracted in the spinach structure [34, 37] which dismissed its previously established role as intrinsic ATPase inhibitor [65-67]. Our assays may help to consolidate those views since some ε-subunit features were also entangled with $\Delta\tilde{\mu}_{H^+}$ [65, 68]. By following the [ATP]/([ADP][Pi]) ratio at thermodynamic equilibrium, we revealed a hampered ATP storage capacity in the *gamera* mutant in extension to its other phenotypes [28, 29]. Likewise, additional independent insights on chloroplast nucleotide transporter regulation may be revealed, which currently rely on fluorescent ATP sensors [32]. Finally, time-resolved characterization of $\Delta\tilde{\mu}_{H^+}$ partitioning may become accessible by describing the $\Delta\tilde{\mu}_{H^+}$ after short illumination periods with our method, as well as thylakoid ion channel/antiporter effects during the photosynthetic induction phase.

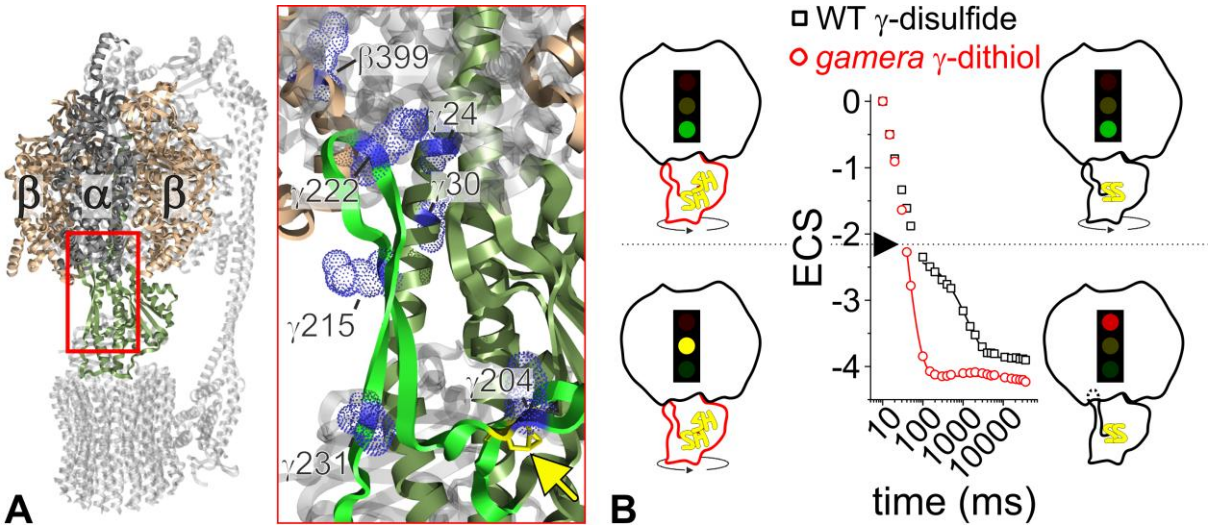

Fig 6: A selection of $\Delta\tilde{\mu}_{H^+}$-dependent structural rearrangements in spinach CF_1F_o and a tentative model for different ATP synthesis rates as a function of $\Delta\tilde{\mu}_{H^+}$ are shown. (A) The structure of spinach CF_1F_o (PDB ID: 6FKH) magnifies the redox loop on the right (light green, arrow pointing to disulfide in yellow sticks). The frontal α-subunit is magnified half-transparent for the sake of visibility of the γ-subunit (dark green). The ATPase choc structure is formed by the γ-hairpin loop around position 222 which is stabilized by the disulfide [34, 37]. A variety of structural rearrangements are depending on the $\Delta\tilde{\mu}_{H^+}$, including the γ-hairpin. Various residues (blue spheres) become available for chemical labeling or trypsin digestion exclusively in illuminated thylakoids [reviewed in 38]. (B) The exposed position of the choc structure in $\Delta\tilde{\mu}_{H^+}$-activated CF_1F_o allows for efficient rotational catalysis in both γ-redox states (top cartoons of subunits $\alpha_3\beta_3\gamma$). Below the WT activation threshold (arrowhead and horizontal line), the disulfide-stabilized choc structure prevents efficient ATP synthesis. The *gamera* sustains an active conformation at this $\Delta\tilde{\mu}_{H^+}$ since the rotating choc structure is less efficiently stabilized inside the $\alpha_3\beta_3$ cavity, owing to the absence of the γ-disulfide.

Acknowledgements:

B.B. and F.B. acknowledge funding from the ERC Starting Grant PhotoPHYTOMICS (ERC-2016-STG grant # 715579). F.B. also acknowledges the CNRS and the “Initiative d' Excellence” Program from the French state grant “DYNAMO”, ANR-11-LABX-0011-01.

Competing interests:

All authors declare no competing interests.

Reference list

[1] U. Armbruster, L.R. Carrillo, K. Venema, L. Pavlovic, E. Schmidtmann, A. Kornfeld, P. Jahns, J.A. Berry, D.M. Kramer, M.C. Jonikas, Ion antiport accelerates photosynthetic acclimation in fluctuating light environments, Nat Commun, 5 (2014) 5439.

[2] A. Herdean, E. Teardo, A.K. Nilsson, B.E. Pfeil, O.N. Johansson, R. Unnep, G. Nagy, O. Zsiros, S. Dana, K. Solymosi, G. Garab, I. Szabo, C. Spetea, B. Lundin, A voltage-dependent chloride channel fine-tunes photosynthesis in plants, Nat Commun, 7 (2016) 11654.

[3] W. Junge, N. Nelson, ATP synthase, Annu. Rev. Biochem., 84 (2015) 631-657.

[4] T. Hisabori, E.I. Sunamura, Y. Kim, H. Konno, The chloroplast ATP synthase features the characteristic redox regulation machinery, Antioxidants & Redox Signaling, 19 (2013) 1846-U1216.

[5] H. Seelert, A. Poetsch, N.A. Dencher, A. Engel, H. Stahlberg, D.J. Muller, Structural biology. Proton-powered turbine of a plant motor, Nature, 405 (2000) 418-419.

[6] R.E. McCarty, J.S. Fuhrman, Y. Tsuchiya, Effects of adenine nucleotides on hydrogen-ion transport in chloroplasts, Proc Natl Acad Sci U S A, 68 (1971) 2522-2526.

[7] G. Groth, W. Junge, Proton slip of the chloroplast ATPase: its nucleotide dependence, energetic threshold, and relation to an alternating site mechanism of catalysis, Biochemistry, 32 (1993) 8103-8111.

[8] P. Turina, J. Petersen, P. Gräber, Thermodynamics of proton transport coupled ATP synthesis, Biochim. Biophys. Acta, 1857 (2016) 653-664.

[9] P. Mitchell, Coupling of phosphorylation to electron and hydrogen transfer by a chemi-osmotic type of mechanism, Nature, 191 (1961) 144-148.

[10] A. Kanazawa, D.M. Kramer, *In vivo* modulation of nonphotochemical exciton quenching (NPQ) by regulation of the chloroplast ATP synthase, Proc. Natl. Acad. Sci. USA, 99 (2002) 12789-12794.

[11] P. Horton, A.V. Ruban, D. Rees, A.A. Pascal, G. Noctor, A.J. Young, Control of the light-harvesting function of chloroplast membranes by aggregation of the LHCII chlorophyll-protein complex, FEBS Lett., 292 (1991) 1-4.

[12] A.V. Ruban, Light harvesting control in plants, FEBS Lett., 592 (2018) 3030-3039.

[13] J.N. Nishio, J. Whitmarsh, Dissipation of the Proton Electrochemical Potential in Intact Chloroplasts (II. The pH Gradient Monitored by Cytochrome f Reduction Kinetics), Plant Physiol., 101 (1993) 89-96.

[14] K. Takizawa, A. Kanazawa, D.M. Kramer, Depletion of stromal Pi induces high 'energy-dependent' antenna exciton quenching (q_E) by decreasing proton conductivity at CFo-CF1 ATP synthase, Plant Cell Environ, 31 (2008) 235-243.

[15] F. Buchert, B. Bailleul, T. Hisabori, A γ-subunit point mutation in *Chlamydomonas reinhardtii* chloroplast F_1F_o-ATP synthase confers tolerance to reactive oxygen species, Biochim. Biophys. Acta, 1858 (2017) 966-974.

[16] W. Junge, B. Rumberg, H. Schroder, The necessity of an electric potential difference and its use for photophosphorylation in short flash groups, Eur. J. Biochem., 14 (1970) 575-581.

[17] W. Junge, The critical electric potential difference for photophosphorylation. Its relation to the chemiosmotic hypothesis and to the triggering requirements of the ATPase system, Eur. J. Biochem., 14 (1970) 582-592.

[18] G. Kaim, P. Dimroth, ATP synthesis by F-type ATP synthase is obligatorily dependent on the transmembrane voltage, EMBO J., 18 (1999) 4118-4127.

[19] J.H. Kaplan, E. Uribe, A.T. Jagendorf, ATP hydrolysis caused by acid-base transition of spinach chloroplasts, Arch Biochem Biophys, 120 (1967) 365-370.

[20] P. Gräber, H.T. Witt, Relations between the electrical potential, pH gradient, proton flux and phosphorylation in the photosynthetic membrane, Biochim. Biophys. Acta, 423 (1976) 141-163.

[21] D.A. Harris, A.R. Crofts, The initial stages of photophosphorylation. Studies using excitation by saturating, short flashes of light, Biochim. Biophys. Acta, 502 (1978) 87-102.

[22] D.M. Kramer, A.R. Crofts, Activation of the chloroplast ATPase measured by the electrochromic change in leaves of intact plants, Biochimica et Biophysica Acta, 976 (1989) 28-41.

[23] P. Joliot, A. Joliot, Quantification of the electrochemical proton gradient and activation of ATP synthase in leaves, Biochim. Biophys. Acta, 1777 (2008) 676-683.
[24] K. Yoshida, A. Hara, K. Sugiura, Y. Fukaya, T. Hisabori, Thioredoxin-like2/2-Cys peroxiredoxin redox cascade supports oxidative thiol modulation in chloroplasts, Proc. Natl. Acad. Sci. USA, 115 (2018) E8296-E8304.
[25] J.D. Mills, P. Mitchell, P. Schurmann, Modulation of coupling factor ATPase activity in intact chloroplasts - The role of the thioredoxin system, FEBS Lett., 112 (1980) 173-177.
[26] B. Naranjo, C. Mignee, A. Krieger-Liszkay, D. Hornero-Mendez, L. Gallardo-Guerrero, F.J. Cejudo, M. Lindahl, The chloroplast NADPH thioredoxin reductase C, NTRC, controls non-photochemical quenching of light energy and photosynthetic electron transport in Arabidopsis, Plant Cell Environ, 39 (2016) 804-822.
[27] L.R. Carrillo, J.E. Froehlich, J.A. Cruz, L.J. Savage, D.M. Kramer, Multi-level regulation of the chloroplast ATP synthase: the chloroplast NADPH thioredoxin reductase C (NTRC) is required for redox modulation specifically under low irradiance, Plant J., 87 (2016) 654-663.
[28] K. Kohzuma, C. Dal Bosco, A. Kanazawa, A. Dhingra, W. Nitschke, J. Meurer, D.M. Kramer, Thioredoxin-insensitive plastid ATP synthase that performs moonlighting functions, Proc. Natl. Acad. Sci. USA, 109 (2012) 3293-3298.
[29] K. Kohzuma, J.E. Froehlich, G.A. Davis, J.A. Temple, D. Minhas, A. Dhingra, J.A. Cruz, D.M. Kramer, The Role of Light-Dark Regulation of the Chloroplast ATP Synthase, Frontiers in Plant Science, 8 (2017) 1248.
[30] D.R. Ort, K. Oxborough, *In situ* regulation of chloroplast coupling factor activity, Annu. Rev. Plant Physiol. Plant Mol. Biol., 43 (1992) 269-291.
[31] G. Wu, D.R. Ort, Mutation in the cysteine bridge domain of the γ subunit affects light regulation of the ATP synthase but not photosynthesis or growth in Arabidopsis, Photosynthesis Res., 97 (2008) 185-193.
[32] C.P. Voon, X. Guan, Y. Sun, A. Sahu, M.N. Chan, P. Gardestrom, S. Wagner, P. Fuchs, T. Nietzel, W.K. Versaw, M. Schwarzlander, B.L. Lim, ATP compartmentation in plastids and cytosol of Arabidopsis thaliana revealed by fluorescent protein sensing, Proc. Natl. Acad. Sci. USA, 115 (2018) E10778-E10787.
[33] J.Z. Pu, M. Karplus, How subunit coupling produces the γ subunit rotary motion in F_1-ATPase, Proc. Natl. Acad. Sci. USA, 105 (2008) 1192-1197.
[34] A. Hahn, J. Vonck, D.J. Mills, T. Meier, W. Kuhlbrandt, Structure, mechanism, and regulation of the chloroplast ATP synthase, Science, 360 (2018).
[35] F. Buchert, H. Konno, T. Hisabori, Redox regulation of CF_1-ATPase involves interplay between the γ-subunit neck region and the turn region of the βDELSEED-loop, Biochim. Biophys. Acta, 1847 (2015) 441-450.
[36] U. Junesch, P. Gräber, Influence of the redox state and the activation of the chloroplast ATP synthase on proton-transport-coupled ATP synthesis hydrolysis, Biochim. Biophys. Acta, 893 (1987) 275-288.
[37] J.H. Yang, D. Williams, E. Kandiah, P. Fromme, P.L. Chiu, Structural basis of redox modulation on chloroplast ATP synthase, Communications biology, 3 (2020) 482.
[38] M.L. Richter, R. Hein, B. Huchzermeyer, Important subunit interactions in the chloroplast ATP synthase, Biochim. Biophys. Acta, 1458 (2000) 326-342.
[39] W. Junge, H.T. Witt, On the ion transport system of photosynthesis--investigations on a molecular level, Z Naturforsch B, 23 (1968) 244-254.
[40] H.T. Witt, Energy conversion in the functional membrane of photosynthesis. Analysis by light pulse and electric pulse methods. The central role of the electric field, Biochim. Biophys. Acta, 505 (1979) 355-427.
[41] B. Bailleul, P. Cardol, C. Breyton, G. Finazzi, Electrochromism: a useful probe to study algal photosynthesis, Photosynthesis Res., 106 (2010) 179-189.

[42] G. Wu, G. Ortiz-Flores, A. Ortiz-Lopez, D.R. Ort, A point mutation in *atpC1* raises the redox potential of the Arabidopsis chloroplast ATP synthase γ subunit regulatory disulfide above the range of thioredoxin modulation, J. Biol. Chem., 282 (2007) 36782-36789.
[43] W. Junge, W. Auslander, A.J. McGeer, T. Runge, The buffering capacity of the internal phase of thylakoids and the magnitude of the pH changes inside under flashing light, Biochim. Biophys. Acta, 546 (1979) 121-141.
[44] C. Lemaire, F.A. Wollman, P. Bennoun, Restoration of phototrophic growth in a mutant of *Chlamydomonas reinhardtii* in which the chloroplast *atpB* gene of the ATP synthase has a deletion: an example of mitochondria-dependent photosynthesis, Proc. Natl. Acad. Sci. USA, 85 (1988) 1344-1348.
[45] J. Reiser, N. Linka, L. Lemke, W. Jeblick, H.E. Neuhaus, Molecular physiological analysis of the two plastidic ATP/ADP transporters from Arabidopsis, Plant Physiol., 136 (2004) 3524-3536.
[46] O. Trentmann, T. Mühlhaus, D. Zimmer, F. Sommer, M. Schroda, I. Haferkamp, I. Keller, B. Pommerrenig, H.E. Neuhaus, Identification of Chloroplast Envelope Proteins with Critical Importance for Cold Acclimation, Plant Physiol., 182 (2020) 1239-1255.
[47] B. Bailleul, N. Berne, O. Murik, D. Petroutsos, J. Prihoda, A. Tanaka, V. Villanova, R. Bligny, S. Flori, D. Falconet, A. Krieger-Liszkay, S. Santabarbara, F. Rappaport, P. Joliot, L. Tirichine, P.G. Falkowski, P. Cardol, C. Bowler, G. Finazzi, Energetic coupling between plastids and mitochondria drives CO_2 assimilation in diatoms, Nature, 524 (2015) 366-369.
[48] D.J. Cline, S.E. Redding, S.G. Brohawn, J.N. Psathas, J.P. Schneider, C. Thorpe, New water-soluble phosphines as reductants of peptide and protein disulfide bonds: reactivity and membrane permeability, Biochemistry, 43 (2004) 15195-15203.
[49] H. Konno, T. Nakane, M. Yoshida, H. Ueoka-Nakanishi, S. Hara, T. Hisabori, Thiol modulation of the chloroplast ATP synthase is dependent on the energization of thylakoid membranes, Plant Cell Physiol., 53 (2012) 626-634.
[50] W. Schliephake, W. Junge, H.T. Witt, Correlation between field formation, proton translocation, and the light reactions in photosynthesis, Z Naturforsch B, 23 (1968) 1571-1578.
[51] A.A. Bulychev, W.J. Vredenberg, Effect of ionophores A23187 and nigericin on the light-induced redistribution of Mg^{2+}, K^+ and H^+ across the thylakoid membrane, Biochim. Biophys. Acta, 449 (1976) 48-58.
[52] P. Bennoun, Chlororespiration revisited: Mitochondrial-plastid interactions in Chlamydomonas, Biochim. Biophys. Acta, 1186 (1994) 59-66.
[53] P.R. Lange, C. Geserick, G. Tischendorf, R. Zrenner, Functions of chloroplastic adenylate kinases in Arabidopsis, Plant Physiol., 146 (2008) 492-504.
[54] A.U. Igamberdiev, L.A. Kleczkowski, Optimization of ATP synthase function in mitochondria and chloroplasts via the adenylate kinase equilibrium, Front Plant Sci, 6 (2015) 10.
[55] V. De Col, P. Fuchs, T. Nietzel, M. Elsässer, C.P. Voon, A. Candeo, I. Seeliger, M.D. Fricker, C. Grefen, I.M. Møller, A. Bassi, B.L. Lim, M. Zancani, A.J. Meyer, A. Costa, S. Wagner, M. Schwarzländer, ATP sensing in living plant cells reveals tissue gradients and stress dynamics of energy physiology, Elife, 6 (2017) e26770.
[56] P.K. Pullela, T. Chiku, M.J. Carvan, 3rd, D.S. Sem, Fluorescence-based detection of thiols in vitro and in vivo using dithiol probes, Anal. Biochem., 352 (2006) 265-273.
[57] R.J. Duhe, B.R. Selman, The dithiothreitol-stimulated dissociation of the chloroplast coupling factor-1 ε subunit is reversible, Biochim. Biophys. Acta, 1017 (1990) 70-78.
[58] R.J. Duhe, B.R. Selman, Studies on the heterogeneity of the soluble chloroplast coupling factor 1: The formation of ε-deficient isozymes, Biochim. Biophys. Acta, 974 (1989) 294-302.
[59] M.L. Richter, W.J. Patrie, R.E. McCarty, Preparation of the ε subunit and ε subunit-deficient chloroplast coupling factor-1 in reconstitutively active forms, J. Biol. Chem., 259 (1984) 7371-7373.
[60] M. Komatsu-Takaki, Energizing effects of illumination on the reactivities of lysine residues of the γ subunit of chloroplast ATP synthase, Eur. J. Biochem., 236 (1996) 470-475.

[61] M. Komatsu-Takaki, Effects of Energization and Substrates on the Reactivities of Lysine Residues of the Chloroplast ATP Synthase β Subunit, Eur. J. Biochem., 228 (1995) 265-270.
[62] S.R. Ketcham, J.W. Davenport, K. Warncke, R.E. McCarty, Role of the γ subunit of chloroplast coupling factor-1 in the light-dependent activation of photophosphorylation and ATPase activity by dithiothreitol, J. Biol. Chem., 259 (1984) 7286-7293.
[63] K. Yoshida, Y. Matsuoka, S. Hara, H. Konno, T. Hisabori, Distinct redox behaviors of chloroplast thiol enzymes and their relationships with photosynthetic electron transport in *Arabidopsis thaliana*, Plant Cell Physiol., 55 (2014) 1415-1425.
[64] G.A. Davis, A. Kanazawa, M.A. Schottler, K. Kohzuma, J.E. Froehlich, A.W. Rutherford, M. Satoh-Cruz, D. Minhas, S. Tietz, A. Dhingra, D.M. Kramer, Limitations to photosynthesis by proton motive force-induced photosystem II photodamage, Elife, 5 (2016).
[65] E.A. Johnson, R.E. McCarty, The carboxyl terminus of the ε subunit of the chloroplast ATP synthase is exposed during illumination, Biochemistry, 41 (2002) 2446-2451.
[66] E.A. Johnson, Altered expression of the chloroplast ATP synthase through site-directed mutagenesis in *Chlamydomonas reinhardtii*, Photosynthesis Res., 96 (2008) 153-162.
[67] J.A. Cruz, B. Harfe, C.A. Radkowski, M.S. Dann, R.E. McCarty, Molecular dissection of the ε subunit of the chloroplast ATP synthase of spinach, Plant Physiol., 109 (1995) 1379-1388.
[68] M. Komatsu-Takaki, Energy-dependent conformational changes in the ε subunit of the chloroplast ATP synthase (CF_oCF_1), J. Biol. Chem., 264 (1989) 17750-17753.